Hydrogen Transfer between Ligands: A Density Functional Study of the Rearrangement of $M(\eta^6\text{-}C_7H_8)_2$ into $M(\eta^7\text{-}C_7H_7)(\eta^5\text{-}C_7H_9)$ [M = Mo, Mo^+, Zr]

Benjamin J. Herbert, Mu-Hyun Baik,† and Jennifer C. Green*

Inorganic Chemistry Laboratory, Department of Chemistry, University of Oxford, South Parks Road, Oxford OX1 3QR, U.K.

Received November 12, 2003

The electronic structure of the family of sandwich complexes $M(\eta^6\text{-}C_7H_8)_2$ and $M(\eta^7\text{-}C_7H_7)(\eta^5\text{-}C_7H_9)$ (M = Mo, Mo^+, Zr) was investigated using density functional theory, and their geometries were accounted for. The mechanism for conversion of $M(\eta^6\text{-}C_7H_8)_2$ into $M(\eta^7\text{-}C_7H_7)(\eta^5\text{-}C_7H_9)$ by hydrogen transfer was investigated, and the experimental trends were reproduced. The neutral Mo species was calculated to have an activation free energy 13 kJ mol^{-1} lower than the cationic Mo^+. The rate-limiting step for the transfer in the neutral molybdenum species is breaking of the C−H bond to form a molybdenum hydride intermediate, which rapidly converts into the rearranged product. The transition state is late on the reaction coordinate, and C−H bond breaking occurs after ring slippage to form an (η^6, η^4) 16-electron species. The cationic molybdenum species has a similar reaction profile. The zirconium species is found to have two competing pathways both with higher activations energies: one with an (η^7,η^5) Zr−H intermediate, the other occurring by direct transfer of the hydrogen without forming Zr−H species. The effect of adding PH_3 to the zirconium system has also been studied, which has the effect of lowering the barrier to the direct transfer of hydrogen between the ligands.

Introduction

Hydrogen transfer between ligands is very common in organometallic chemistry[1−3] and can be reversible[4] or irreversible.[5,6] Deriving a mechanistic understanding of such processes on an electronic level is challenging. Thus, although there is now widespread agreement that intramolecular rearrangements of this type are responsible for some chain termination processes in single-site polymerization processes,[7] the exact role of the transition metal in promoting the ligand-based reactions is not well understood. In principle, the mechanism for the hydrogen transfer can be either via an intermediate metal hydride, in an oxidative-addition-like process, or via a direct transfer between the ligands, in a metathesis-like process. It is often difficult to distinguish between the two processes in mechanistic studies, as the intermediates formed after oxidative addition may be short-lived and usually cannot be directly observed.

Intramolecular hydrogen transfer reactions often occur in organometallic compounds to form a thermodynamically more stable species. This is frequently observed in systems with unsaturated ligands that rearrange to generate Hückel aromatic ligands[8] or have greater conjugation of double bonds.[9] Initially many of these reactions were observed in metal vapor synthesis, where the condensed products contained organometallic species with rearranged ligands.[8,9] Gaseous metal atoms were also found to catalyze disproportionation of cyclic polyenes, via formation of organometallic intermediates that were not isolated.[10] Green et al. were the first to isolate $Mo(\eta^6\text{-}C_7H_8)_2$ via reaction of molybdenum atoms with cycloheptatriene,[11] the first example of a metal atom cycloheptatriene complex formed in this way. Previous attempts had always formed rearranged compounds, where a hydride shift had occurred to form $M(\eta^7\text{-}C_7H_7)(\eta^5\text{-}C_7H_9)$.[8,10,12] $Mo(\eta^6\text{-}C_7H_8)_2$ was found to undergo quantitative isomerization in the solid state or solution to give the previously isolated compound $Mo(\eta^7\text{-}C_7H_7)(\eta^5\text{-}C_7H_9)$. Fortuitously, the kinetics of the isomerization were suitable for mechanistic study, with a half-life of 200 h at room temperature. The rearrangement was shown to be intramolecular, with a rate almost independent of solvent polarity.[13] Interestingly,

* Corresponding author. E-mail: jennifer.green@chem.ox.ac.uk.
† Current address: Department of Chemistry, 800 E. Kirkwood Ave., Bloomington, IN 47405.

(1) Tolman, C. A. *Transition Metal Hydrides*; New York, 1971.
(2) Hubert, A. J.; Reimlinger, H. *Synthesis* **1970**, *2*, 405.
(3) Gorewit, B.; Tsutsui, M. *Adv. Catal.* **1978**, *27*, 227−263.
(4) Brookhart, M.; Green, M. L. H.; Pardy, R. B. A. *J. Chem. Soc., Chem. Commun.* **1983**, 691−693.
(5) Pertici, P.; Simonelli, G.; Vitulli, G.; Deganello, G.; Sandrini, P.; Mantovani, A. *J. Chem. Soc., Chem. Commun.* **1977**, 132−133.
(6) Itoh, K.; Nagashima, H.; Ohshima, T.; Oshima, N.; Nishiyama, H. *J. Organomet. Chem.***1984**, *272*, 179−188.
(7) Stehling, U.; Diebold, J.; Kirsten, R.; Roell, W.; Brintzinger, H. H.; Juengling, S.; Muelhaupt, R.; Langhauser, F. *Organometallics* **1994**, *13*, 964−970.
(8) Van Oven, H. O.; De Liefde Meijer, H. J. *J. Organomet.Chem.* **1971**, *31*, 71−74.
(9) Cable, R. A.; Green, M.; Mackenzie, R. E.; Timms, P. L.; Turney, T. W. *J.Chem. Soc., Chem. Commun.* **1976**, 270−271.
(10) Van Dam, E. M.; Brent, W. N.; Silvon, M. P.; Skell, P. S. *J. Am. Chem. Soc.* **1975**, *97*, 465−467.
(11) Green, M. L. H.; Newman, P. A. *J. Chem. Soc., Chem. Commun.* **1984**, 816−817.
(12) Blackborow, J. R.; Hildenbrand, K.; Von Gustorf, E. K.; Scrivanti, A.; Eady, C. R.; Ehntolt, D.; Krueger, C. *J. Chem. Soc., Chem. Commun.* **1976**, 16−17.

10.1021/om034292z CCC: $27.50
Publication on Web 04/22/2004

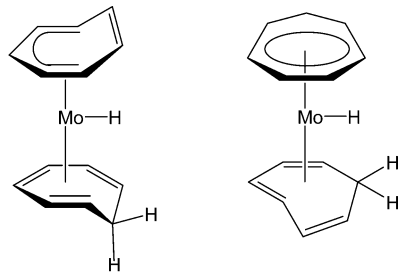

1 2

Figure 1. Proposed structures for the molybdenum hydride intermediate in the conversion of $Mo(C_7H_8)_2$ into $Mo(C_7H_7)(C_7H_9)$.

the 17-electron cationic molybdenum complex was found to have a slower rate of isomerization than the neutral species. Furthermore, the analogous 16-electron zirconium species was found not to isomerize in solution, unless in the presence of a Lewis base.[14] In a classical bonding sense, the driving force of the rearrangement is the formation of the coordinated tropylium ($C_7H_7^+$) cation, suggesting that the hydrogen transfer may be viewed as a hydride shift between ligands. If this were the case, then the rate might be expected to increase as electrons are removed from the metal center. Green et al. concluded that the molybdenum system proceeded via a molybdenum hydride species, in which ring slippage had occurred to keep the electron count at 18 or below. From the kinetic data they were unable to differentiate between 1 or 2 shown in Figure 1 as intermediate structures. The timing of the reaction is also unknown, as it may occur via slow irreversible formation of a molybdenum hydride, which rapidly rearranges, or via a fast preequilibrium that favors the bis-cycloheptatriene complex.

$$[Mo(C_7H_8)_2] \xrightarrow{\text{slow}} [Mo{-}H] \xrightarrow{\text{fast}} [Mo(C_7H_7)(C_7H_9)]$$

$$[Mo(C_7H_8)_2] \overset{\text{fast}}{\rightleftharpoons} [Mo{-}H] \xrightarrow{\text{slow}} [Mo(C_7H_7)(C_7H_9)]$$

Both mechanisms would have a low undetectable concentration of molybdenum hydride and, thus, fit the available data.[13]

We have investigated the system using high-level density functional theory (DFT) to determine the mechanism involved in the rearrangement and to explain the unusual dependence of the reaction rate on the electron count on the metal. The main goal of this study is to provide a detailed conceptual proposal for how the transition metal center promotes the intramolecular hydride transfer.

Computational Methods

Calculations were performed using either Gaussian 98,[15] Jaguar 5.5,[16] or ADF version 2002.02[17−19] to take advantage of the technical differences in these three software packages. ADF was employed for fragment calculations in order to determine the bonding in the stationary points found, and linear transits were used to explore the potential energy surface for possible rearrangement pathways. Jaguar and Gaussian were used for their superior transition state search algorithms, as we found most transition state geometries would not converge using ADF. While the final results obtained with these three programs are largely consistent with each other, there are notable differences in the technical performances. By making use of all three implementations of DFT, we were able to explore the potential energy surface of the reaction more carefully and avoid misleading numerical artifacts.

Gaussian 98 calculations were performed using the density functional/Hartree−Fock hybrid B3LYP.[20−23] Optimizations, solvent correction, and frequency calculations were done with the LanL2DZ[24] basis set for Mo and Zr modified by inclusion of 5p functions,[25] and the 6-31G** basis set was employed for all other atoms. The energies of the stationary points were reevaluated using the Stuttgart−Dresden basis set for the metal, with Dunning's[26] correlation-consistent double-ζ cc-pVDZ basis set for carbon and hydrogen. Transition states were found using the QST2/QST3 method, and all stationary points were verified using frequency calculations. IRC calculations were carried out to verify that the transition states found were correct saddle points connecting the proposed minima. The calculation of solvent effects was performed using the PCM[27−29] model.

Jaguar calculations were performed using the B3LYP functional. Geometry optimizations and solvent and frequency calculations were performed using the 6-31G** basis set, with the metal represented by the Los Alamos LACVP**[24,30,31] basis set. The energies of the optimized structures are reevaluated by additional single-point calculations on each optimized geometry by use of Dunning's[26] correlation-consistent triple-ζ

(13) Green, M. L. H.; Newman, P. A.; Bandy, J. A. *J. Chem. Soc., Dalton Trans.* **1989**, 331−343.
(14) Green, J. C.; Green, M. L. H.; Walker, N. M. *J. Chem. Soc., Dalton Trans.* **1991**, 173−180.
(15) Frisch, M. J.; Trucks, G. W.; Schlegel, H. B.; Scuseria, G. E.; Robb, M. A.; Cheeseman, J. R.; Zakrzewski, V. G.; Montgomery, J. A., Jr.; Stratmann, R. E.; Burant, J. C.; Dapprich, S.; Millam, J. M.; Daniels, A. D.; Kudin, K. N.; Strain, M. C.; Farkas, O.; Tomasi, J.; Barone, V.; Cossi, M.; Cammi, R.; Mennucci, B.; Pomelli, C.; Adamo, C.; Clifford, S.; Ochterski, J.; Petersson, G. A.; Ayala, P. Y.; Cui, Q.; Morokuma, K.; P. S., Dannenberg, J. J.; Malick, D. K.; Rabuck, A. D.; Raghavachari, K.; Foresman, J. B.; Cioslowski, J.; Ortiz, J. V.; A. G. B.; Stefanov, B. B.; Liu, G.; Liashenko, A.; Piskorz, P.; Komaromi, I.; Gomperts, R.; Martin, R. L.; Fox, D. J.; Keith, T.; Al-Laham, M. A.; Peng, C. Y.; Nanayakkara, A.; Challacombe, M.; Gill, P. M. W.; Johnson, B. G.; Chen, W.; Wong, M. W.; Andres, J. L.; Gonzalez, C.; Head-Gordon, M.; Replogle, E. S.; Pople, J. A. *Gaussian 98*, revision A.11.1; Gaussian Inc.: Pittsburgh, PA, 2001.
(16) *Schrödinger*, 5.5 ed.; Schrödinger, 1991−2003.
(17) Baerends, E. J.; Autschbach, J. A.; Berces, A.; Bo, C.; Boerringter, P. M.; Cavallo, L.; Chong, D. P.; Deng, L.; Dickson, R. M.; Ellis, D. E.; Fan, L.; Fischer, T. H.; Fonseca-Guerra, C.; van Gisbergen, S. J.; Groeneveld, J. A.; Gritsenko, O. V.; Grüning, M.; Harris, F. E.; van den Hoek, P.; Jacobsen, H.; van Kessel, G.; Kootstra, F.; van Lenthe, E.; Osinga, V. P.; Patchkovskii, S.; Philipsen, P. H. T.; Post, D.; Pye, C. C.; Ravenek, W.; Ros, P.; Schipper, P. R. T.; Schreckenbach, G.; Snijiders, J. G.; Sola, M.; Swart, M.; Swerhone, D.; te Velde, G.; Vernooijis, P.; Versluis, L.; Visser, O.; van Wezenbeek, E.; Wiesenekker, G.; Wolff, S. K.; Woo, T. K.; Ziegler, T. *ADF* version 2002.02 ; Scientific Computing & Modelling NV: Vrije Universiteit, Amsterdam, 2002.
(18) Velde, G. T.; Bickelhaupt, F. M.; Baerends, E. J.; Guerra, C. F.; Van Gisbergen, S. J. A.; Snijders, J. G.; Ziegler, T. *J. Comput. Chem.* **2001**, *22*, 931−967.
(19) Guerra, C. F.; Snijders, J. G.; te Velde, G.; Baerends, E. J. *Theor. Chem. Acc.* **1998**, *99*, 391−403.
(20) Vosko, S. H.; Wilk, L.; Nusair, M. *Can. J. Phys.* **1980**, *58*, 1200−1211.
(21) Stephens, P. J.; Devlin, F. J.; Chabalowski, C. F.; Frisch, M. J. *J. Phys. Chem.* **1994**, *98*, 11623−11627.
(22) Lee, C.; Yang, W.; Parr, R. G. *Phys. Rev. B: Condens. Matter Mater. Phys.* **1988**, *37*, 785−789.
(23) Becke, A. D. *J. Chem. Phys.* **1993**, *98*, 5648−5652.
(24) Hay, P. J.; Wadt, W. R. *J. Chem. Phys.* **1985**, *82*, 299−310.
(25) Couty, M.; Hall, M. B. *J. Comput. Chem.* **1996**, *17*, 1359−1370.
(26) Dunning, T. H., Jr. *J. Chem. Phys.* **1989**, *90*, 1007−1023.
(27) Miertus, S.; Scrocco, E.; Tomasi, J. *Chem. Phys.* **1981**, *55*, 117−129.
(28) Miertus, S.; Tomasi, J. *Chem. Phys.* **1982**, *65*, 239−245.
(29) Cossi, M.; Barone, V.; Cammi, R.; Tomasi, J. *Chem. Phys. Lett.* **1996**, *255*, 327−335.
(30) Hay, P. J.; Wadt, W. R. *J. Chem. Phys.* **1985**, *82*, 270−283.
(31) Wadt, W. R.; Hay, P. J. *J. Chem. Phys.* **1985**, *82*, 284−298.

basis set cc-pVTZ(-f) that includes a double set of polarization functions. For the metal we have used a modified version of the LACVP**, designated as LACV3P**, where the exponents were decontracted to match the effective core potential with the triple-ζ quality basis.

ADF calculations were performed using Vosko, Wilke, and Nusair's local functional,[20] with the Becke 88[32,33] and the Perdew 86[34] nonlocal exchange and correlation gradient corrections. The basis sets used were uncontracted triple-ζ Slater-type orbitals (STOs). Hydrogen, carbon, and oxygen were given extra polarization functions (2p on H and 3d on C and O). The cores of atoms were frozen, C and O up to the 1s level, and Zr and Mo up to the 3d level. Scalar ZORA relativistic corrections[35−39] were used. Where possible, minima were characterized by full frequency calculations;[40,41] however not all of the proposed minima found using ADF could be verified with this technique, and some structures contained low-energy negative modes corresponding to movements of the rings. All quoted electronic structure data from optimized structures, single-point energy, and fragment calculations use an integration of 6.0 and have gradient corrections applied during the SCF cycles. Linear transit calculations (and the data quoted from their outputs) had gradient corrections applied post SCF convergence and use an integration of 4.0 to increase computational efficiency. During a linear transit, one or more internal variables (internuclear distance or angle) were fixed to successive values as a reaction coordinate and all other variables were optimized to a level of 10^{-2} au/Å (gradient), 10^{-2} Å (bond length), and 0.5° (bond/torsional angle). Calculations of solvent effects were performed using the COSMO model implemented into ADF by Pye and Ziegler.[42] The calculation was done on the solvent-excluding surface using the default radii for the program. The effect of ring bending was determined by defining a dummy atom as the centroid of the six vinyl carbons of the cycloheptatrienyl rings and performing single-point calculations with varying angles subtended by the metal and the two ring centroids. In this way, the inter-ring angle can be varied without changing the metal−carbon bond distances. Ring rotations were achieved by placing dummy atoms defined as the centroid of the six vinyl carbons of the cycloheptatrienyl rings. The torsional angle formed between these and two corresponding carbons on different cycloheptatrienyl rings was then used as a crank to force ring rotation about 180° in 9° steps.

To investigate how the hydrogen is transferred between ligands, linear transits were performed using ADF to ascertain energy profiles for certain rearrangements. Structures along these linear transits were then used as inputs into QST2 and QST3 calculations in Jaguar and Gaussian to locate the transition states. Initially, suitable linear transits moved the hydrogen toward the metal center or directly to the other ring. Timings of the rearrangement processes were found from IRC calculations in Gaussian.

To improve the accuracy of the predicted activation energies, a series of corrections were added. First a larger basis set was used in Gaussian and Jaguar. Next zero-point-energy, thermal energy, and entropy corrections were added to give a gas phase free energy, and finally corrections for the solvent were added to give a solution phase activation energy.

Orbital pictures are drawn at the 95% surface, as produced by the MOLEKEL program.[43]

Data calculated with Gaussian are labeled using the prefix g, and data calculated with Jaguar with the prefix j, to distinguish them from Amsterdam Density Functional (ADF) results (no prefix). Previously known structures are named according to their ring hapticities, M66 referring to a bis-η^6-cycloheptatriene complex, M75 to M(η^7-C_7H_7)(η^5-C_7H_9), where M = Zr or Mo. Intermediates and transition states are labeled according to the order they appear when converting M66 into M75. Orbitals are numbered according to their levels in ADF.

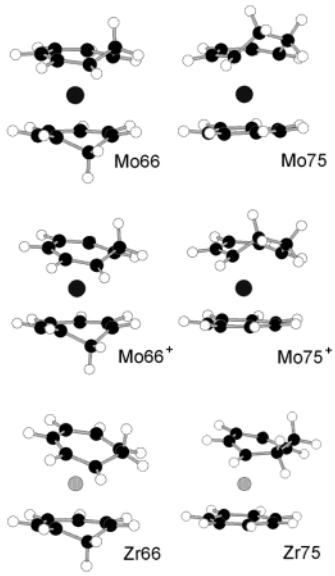

Figure 2. Optimized structures found using ADF for the known compounds M66 and M75 (M = Mo, Mo^+, Zr).

Table 1. Average Geometrical Data for the Known Stationary Points of M66 Found Using ADF, and Data for the Crystal Structure of Zr66[a]

	Mo66	$Mo66^+$	Zr66	Zr66 (X-ray)
av C−C	1.418	1.420	1.422	1.409
av M−C	2.333	2.341	2.460	2.422
ring angle α	7.3	15.1	25.6	26.8
ring torsion β	46.6	48.5	45.6	45.6

[a] α is the angle between the two planes formed by three atoms in each ring. β is the torsion angle between two identical ring carbons through a dummy atom at the midpoint of the rings.

Results and Discussion

Structures of M66 and M75. Calculated structures for the known compounds Mo66, Mo75, $Mo66^+$, $Mo75^+$, Zr66, and Zr75 are shown in Figure 2, and geometrical data are given in Tables 1 and 2. The structures were optimized under no symmetry constraints, and in all cases with M66 the converged structures were found to have C_2 symmetry, with a ring torsional angle, β, of approximately 46° from being perfectly eclipsed; this value does not vary significantly between the structures. The ring bending angle, α (defined as the angle between the ring planes), increases as the electron count on the metal decreases; the variation is more pronounced in the M66 series than the M75. Comparing the bond

(32) Becke, A. D. *Phys. Rev. A: At., Mol., Opt. Phys.* **1988**, *38*, 3098−3100.
(33) Becke, A. D. *J. Chem. Phys.* **1988**, *88*, 1053−1062.
(34) Perdew, J. P. *Phys. Rev. B* **1986**, *33*, 8800.
(35) Vanlenthe, E.; Baerends, E. J.; Snijders, J. G. *J. Chem. Phys.* **1993**, *99*, 4597−4610.
(36) Vanlenthe, E.; Baerends, E. J.; Snijders, J. G. *J. Chem. Phys.* **1994**, *101*, 9783−9792.
(37) vanLenthe, E.; Snijders, J. G.; Baerends, E. J. *J. Chem. Phys.* **1996**, *105*, 6505−6516.
(38) vanLenthe, E.; vanLeeuwen, R.; Baerends, E. J.; Snijders, J. G. *Int. J. Quantum Chem.* **1996**, *57*, 281−293.
(39) van Lenthe, E.; Ehlers, A.; Baerends, E. J. *J. Chem. Phys.* **1999**, *110*, 8943−8953.
(40) Fan, L.; Ziegler, T. *J. Phys. Chem.* **1992**, *96*, 6937−6941.
(41) Fan, L.; Ziegler, T. *J. Am. Chem. Soc.* **1992**, *114*, 10890−10897.
(42) Pye, C. C.; Ziegler, T. *Theor. Chem. Acc.* **1999**, *101*, 396−408.
(43) Flukiger, P.; H. P. L.; Portmann, S.; Weber, J. *MOLEKEL*; Swiss Centre for Scientific Computing: Manno, Switzerland, 2000.

Table 2. Average Geometrical Data for the Known Stationary Points of M75 Found Using ADF, and Data for the Crystal Structure of Mo75

	Mo75	Mo75 (X-ray)	$Mo75^+$	Zr75
η^5 ring				
av C−C	1.424	1.396	1.423	1.417
av M−C	2.346	2.321	2.356	2.545
η^7 ring				
av C−C	1.423	1.388	1.424	1.432
av M−C	2.311	2.255	2.318	2.398
ring angle α[a]	3.6	5.8	9.1	19.4

[a] α is the angle between the two planes formed by three atoms in each ring.

length data for the M75 structures, the average coordinated C−C bond lengths do not differ between the η^5 and η^7 rings (except only slightly with Zr), but the average M−C bond lengths do differ significantly. The M−C bond lengths are around 0.04 Å shorter to the η^7 ring for Mo and Mo^+ and over 0.1 Å shorter for Zr. Jaguar and Gaussian gave similar results.

Bonding in M66 and M75. MO Analysis. Bonding in both these sandwich compounds can be regarded as a perturbation on that of a classic metallocene in which the MOs are classified as σ, π, and δ with respect to the metal ring axis. The metal-based σ HOMO is principally d(z^2) and nonbonding. The π orbitals correspond to ligand−metal donation and are principally ligand in character, and the δ orbitals to metal−ligand back-donation, being mainly metal in character. For a d^6, 18-electron molecule three metal orbitals, one of σ and two of δ symmetry, are occupied.

The MO diagrams for Mo66 and Mo75 are shown in Figure 3. Analysis of the frontier orbitals in Mo66 and Mo75 show that both have a nonbonding metal-centered HOMO, 43, of σ symmetry, deriving from the Mo d(z^2) orbital. The δ orbitals, 42 and 41, are near degenerate in Mo66, but are separated in energy in Mo75; they derive from the metal d(xy) and d(x^2-y^2) orbitals mixed with empty orbitals on the ligands.

Mo66 has four orbitals of π symmetry with respect to the metal−ring axis, 40, 39, 38, and 37. The originating ring orbitals $6\pi_2$ and $6\pi_3$ differ in energy as the contributing η^6 rings have lobes that are either bonding, $6\pi_3$, or antibonding, $6\pi_2$, across the open end of the π system. The upper pair 40 and 39 are $6\pi_3$ based, while the more stable pair, 38 and 37, are $6\pi_2$ based.

In Mo75 the aromatization of C_7H_7 makes the η^7-ring π orbitals degenerate, and they lower in energy significantly. The poor δ-acceptors in the η^5 fragment hardly participate in the bonding in orbitals 42 and 41, although they make some contribution to orbital 42. Orbital 41 is lower in energy, as it bonds mainly to the η^7 ring. The energies of the π orbitals are determined by their ligand origin. Orbitals 40 and 39 are split apart and are mainly based on the η^5 ring; the splitting is due to the poor bonding in $5\pi_3$, which has a diffuse bonding lobe across the open face of the C_7H_9 fragment. The other π orbitals, 37 and 36, are significantly lower in energy and drop below orbital 38, giving two π symmetry bonding orbitals primarily $7\pi_2$ and $7\pi_3$ in character with little contribution from the η^5 ring. Orbital 38 is of $5\pi_1$ origin. In changing from Mo66 to Mo75, the amount of metal character decreases in the lower pair of π bonding orbitals. This is consistent with the proposed driving force for the rearrangement being aromatization of the C_7H_7 ring.

$Mo66^+$ and $Mo75^+$ have very similar orbital structures, the principal difference being that orbital 43 is only half-occupied.

The orbital assignment in Zr66 is similar to that in Mo66, with the HOMO now being the δ-bonding orbital 42. The crystal structure shows an unusual alternation in bond lengths in the metal to ring carbon bonds, with two carbons on each ring being ∼0.05 Å closer to the metal. This is not observed in our calculated structure, where all Zr−C distances are approximately equal. However comparison of the structure with the filled bonding orbitals of Zr66 shows the shorter metal carbon bonds correspond perfectly to the bonding lobes in orbital 41, so the experimental structure can be rationalized. A previously published calculated structure[44] using a DZ quality basis set found the Zr−C bond lengths to vary around the ring; however their results also did not correlate with the alternations observed in the crystal structure.

In all cases the total energy of M75 is lower than M66, showing a clear thermodynamic driving force for the rearrangement to take place. $Mo75^+$ and Zr75 have a stabilization of ∼35 kJ mol^{-1}, while Mo75 is stabilized by 64.6 kJ mol^{-1}. The relative greater stability of Mo75 compared to Mo75+ can be attributed to the stronger δ bonds formed by the neutral metal.

The C_7H_7 fragment is formally classified as $C_7H_7^+$; thus M in M75 is in the 0 oxidation state. Aromaticity can also be achieved by forming a 3^- ligand, which would formally involve oxidation of the metal to form M(IV). Analysis of the Mulliken and multipole derived charges[45] (the charge on the metal atom for the various structures can be found in the Supporting Information) reveals there is very little change in the charge on the metal between the two structures, indicating that the metal is unlikely to have undergone oxidation.

Ring Bending. Because the main structural difference between the three pairs of compounds was the angle between the ring planes, the effect of varying this angle was studied. The results for Mo66 are shown in Figure 4. The total energy of this 18-electron compound was found to increase significantly with inter-ring angle. Orbitals 43 and 40 increase in energy on bending, while orbitals 42, 41, and 39 exhibit a decrease in energy, with a minimum at an inter-ring angle of approximately 35°. Orbital 43 exerts a strong preference for the rings to be parallel; hence in Mo66, where this orbital is doubly occupied, the inter-ring angle is observed to be close to 0°. Removing an electron from orbital 43 reduces the effect it has on the structure of the complex, and so $Mo66^+$ has a larger inter-ring angle than Mo66, while in Zr66, where orbital 43 is empty, the inter-ring angle is the largest for the three compounds.

Calculations were also performed to model bending in Mo75. It was found again that orbital 43 significantly increases in energy on ring bending, while orbitals 42 and 39 lower in energy on ring bending. The energy change in orbitals 42 and 39 is smaller than that found

(44) Jarrett-Sprague, S. A.; Hillier, I. H. *Int J. Mass Spectrom. Ion Processes* **1992**, *122*, 349−359.
(45) Swart, M.; Van Duijnen, P. T.; Snijders, J. G. *J. Comput. Chem.* **2000**, *22*, 79−88.

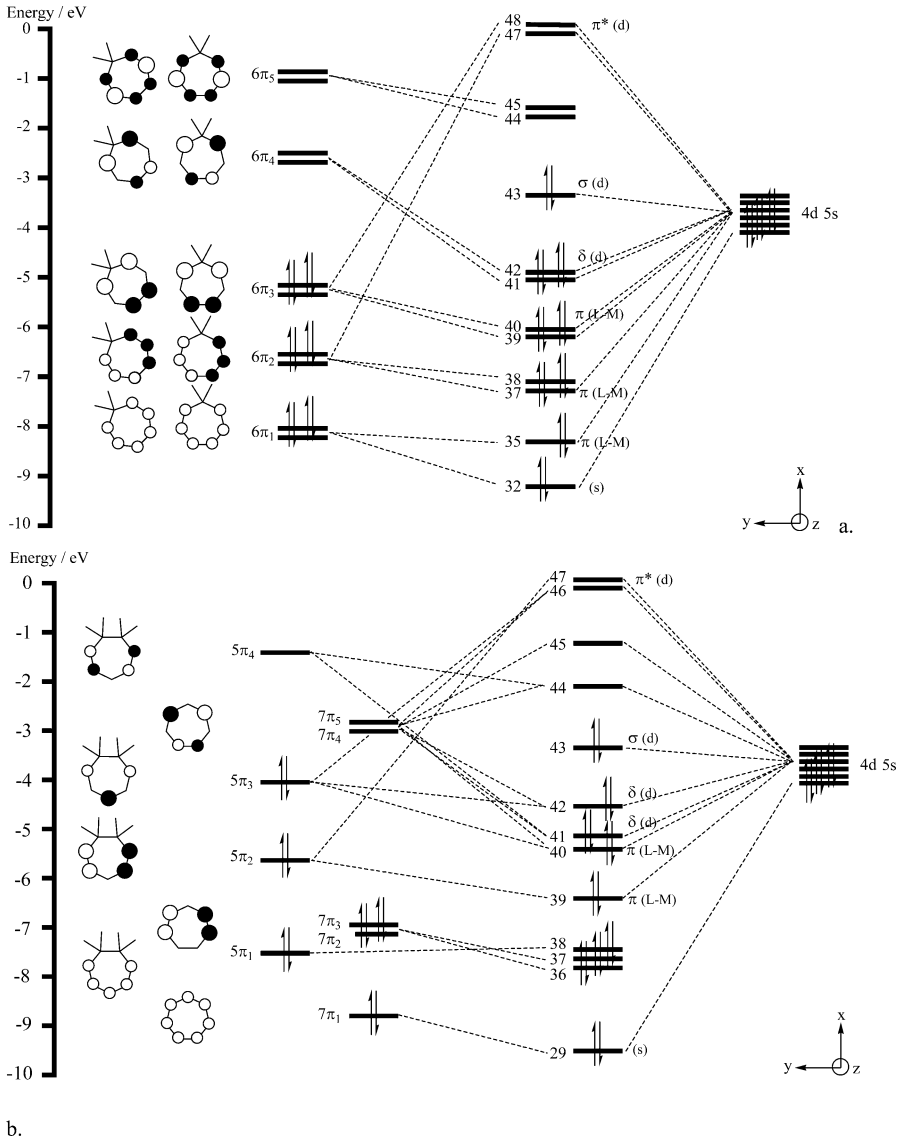

Figure 3. MO diagrams of Mo66 (a) and Mo75 (b) taken from ADF fragment calculations. The left-hand side shows the energy levels of the π orbitals of the ring fragments, labeled according to the ring hapticities: 5π is η^5-C_7H_9, 6π is η^6-C_7H_8, and 7π is η^7-C_7H_7. The η^5 and η^7 rings have been calculated as spin-restricted neutral fragments.

in Mo66, as bending only improves the bonding to the η^5 ring as opposed to both rings in Mo66. This accounts for the smaller inter-ring angle observed in M75 systems.

Ring Rotations in Mo66. The crystal structure of Mo66 shows a 7-fold positional disorder of the methylene group due to ring rotations, so the lowest energy conformation for the relative position of the two methylene groups is not known.[13] VT NMR experiments show the two rings are rotating relative to one another at room temperature, with a barrier to rotation estimated at 50.7 ± 0.7 kJ mol^{-1}.[13] A linear transit was performed to reproduce the energy profile of ring rotation, as shown in Figure 5a.

C_2 symmetry of the complex leads to the profile for angles 180−360° being the mirror image of that given in Figure 5a. Thus there are four energy minima associated with the full rotation. Structure D was optimized in ADF and a frequency calculation performed to verify it as a true minimum. It was found to have an energy 4.8 kJ mol^{-1} lower than the energy found for the structure shown in Figure 2 (conformation B). Optimizing the transition state structures A and C without any bond constraints found them 77.8 and 63.2 kJ mol^{-1} higher in energy than D, respectively, which gives an activation energy to ring rotation in reasonable agreement with the experimental value of 50.7 kJ mol^{-1}.

Figure 5b shows the progression of the occupied frontier orbitals during the ring rotations linear transit. The HOMO (orbital 43) remains at approximately constant energy, reflecting its nonbonding character, whereas orbitals 42 and 41 vary across the transit. The energy of 42 correlates well with the total energy given in Figure 5a, suggesting it is the major factor in ring conformation. Green et al. stated that at A the molecule has C_{2v} symmetry, and only one of the d δ orbitals has the correct symmetry to back-donate to the b_2 combination of $6\pi_4$.[14] Structure C has the same symmetry as B and D, so this symmetry argument is no longer valid. In a C_2 point group, the ring orbitals of equivalent energies combine to make an A and B symmetry combination. The two δ symmetry d orbitals of molybdenum also transform as an A and B symmetry combination. At the maxima in Figure 5a, with an inter-

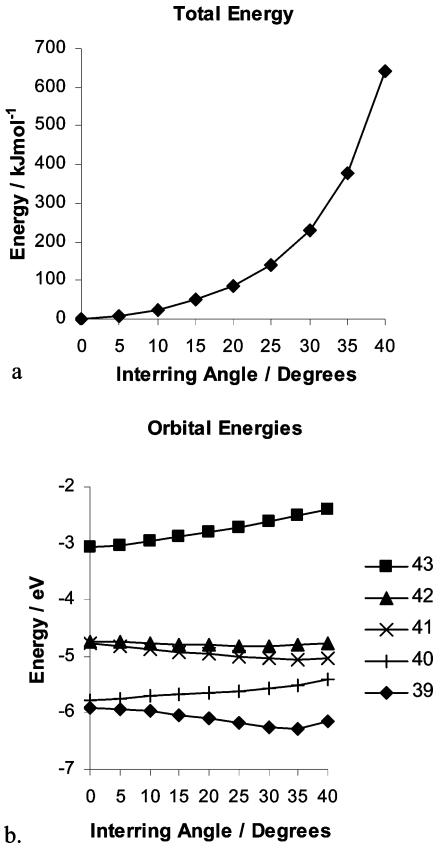

Figure 4. Effect of varying γ (180° − angle between metal atom and two ring centroids) in Mo66 on (a) the total energy and (b) orbital energies.

ring angle of 0°, 90°, and 180°, the spatial orientation of the orbitals means one of the combinations of the $6\pi_4$ orbitals is not able to accept back-donation from the metal. This means a combination from the $6\pi_5$ orbitals must participate in back-donation. Conversely at the minimum energy conformations, both the A and B symmetry combination formed from $6\pi_4$ are able to interact with the metal orbitals. As the $6\pi_4$ orbitals are significantly lower in energy, they are more favorable for back-donation from the metal. This difference is shown schematically in Figure 6.

Transformation of Mo66 into Mo75. The experimental activation energy for the hydride shift in Mo66 is on the order 100 kJ mol^{-1}. This lies well above the energy needed for ring rotation, so it can be assumed that ring rotation does not act as the rate-determining step in hydride transfer. It is reasonable to assume the hydrogen would move directly to form a 1,3-cycloheptadienyl moiety, rather than a 1,4-cycloheptadienyl which then undergoes another H-shift, as there is no kinetic or spectroscopic evidence of any other isomers of Mo(C_7H_7)(C_7H_9) being involved. All further discussion will therefore focus on the structure and reaction of conformer B, which is suitably orientated to allow a direct H-shift between ligands.

The total energy required for a direct transfer of hydrogen was calculated to be on the order 350 kJ mol^{-1} in Mo66, which is so far above the experimental activation energy that the direct hydride migration without mediation by the metal may be ruled out. The principal barrier to the process is the energy required for bending the rings to a geometry where direct transfer can take place.

A reaction pathway for H migration was identified. Figure 7a shows the stationary points found using ADF, Gaussian, and Jaguar. Two intermediates and three transition states were identified on the reaction pathway. In the first intermediate, Int1, the upper cycloheptatriene ring has decoordinated to form an η^4,η^7 complex, and a distinct Mo−H bond formed. The second intermediate, Int2, is also an η^4,η^7 complex, in which the migrating hydride has formed a bond to the upper ring and is now agostically bonded to the metal. Comparison of the stationary points found using the different software packages shows they are in general in excellent agreement. Figure 7b shows the relative free energies for the structures shown in Figures 2 and 7a. The rate-determining step is the formation of the molybdenum hydride species Int1. This is in agreement with the mechanism proposed by Green et al. from their kinetic data.[13] The transition state for migration of the transferring hydrogen to the metal was identified using both Gaussian and Jaguar. The predicted activation energy of 162 kJ mol^{-1} (Jaguar) is significantly higher than the experimentally determined value of 101 kJ mol^{-1};[13] however it is in better agreement than the values determined from the direct transfer between ligands. A single-point calculation in ADF of the structure gTS1 gave an activation energy of 129.7 kJ mol^{-1}, which is closer to the experimental value. A frequency calculation on the structure in ADF revealed two imaginary normal modes, one at 654i cm^{-1} corresponding to the motion along the reaction coordinate, and another at 105i cm^{-1} corresponding to a small movement of the decoordinated olefin. The structure gTS1 does not exactly correspond to the (undiscovered) ADF transition state; however it is likely to be close in energy. These activation energies become significantly lowered on adding the corrections for basis set, zero-point energy, thermal energy, and solvent, the relative activation barriers being 96 kJ mol^{-1} for ADF, 106.3 kJ mol^{-1} for Gaussian, and 122.8 kJ mol^{-1} for Jaguar at 298.15 K. The Gaussian and ADF results are in very good agreement with the experimentally observed activation free energy of 103 ± 3 kJ mol^{-1}.[13] Table 3 details the effect of the corrections on the relative energies of Mo66 and TS1. It is noteworthy that inclusion of the zero-point and thermal energies gives the most significant improvement in activation energy. In forming the transition state, a C−H bond is being broken, to give a species with a loosely bound hydrogen atom. The transition state is therefore expected to have several lower frequency vibrational modes which will give a smaller zero-point energy than the ground state and will contribute less when populated with thermal energy.

The structure of jTS1 in Figure 7a shows ring slippage has almost completely occurred, and the C−H bond is significantly lengthened at 1.398 Å. Both these factors suggest the transition state lies very late in the path between Mo66 and Int1, with the C−H bond breaking being the highest energy step. Green et al. reported an experimental kinetic isotope effect of the perdeuterio analogue $k_H/k_D = 2.16 \pm 0.3$ at 313.5 K.[13] Frequency calculations were performed on the perdeuterio ana-

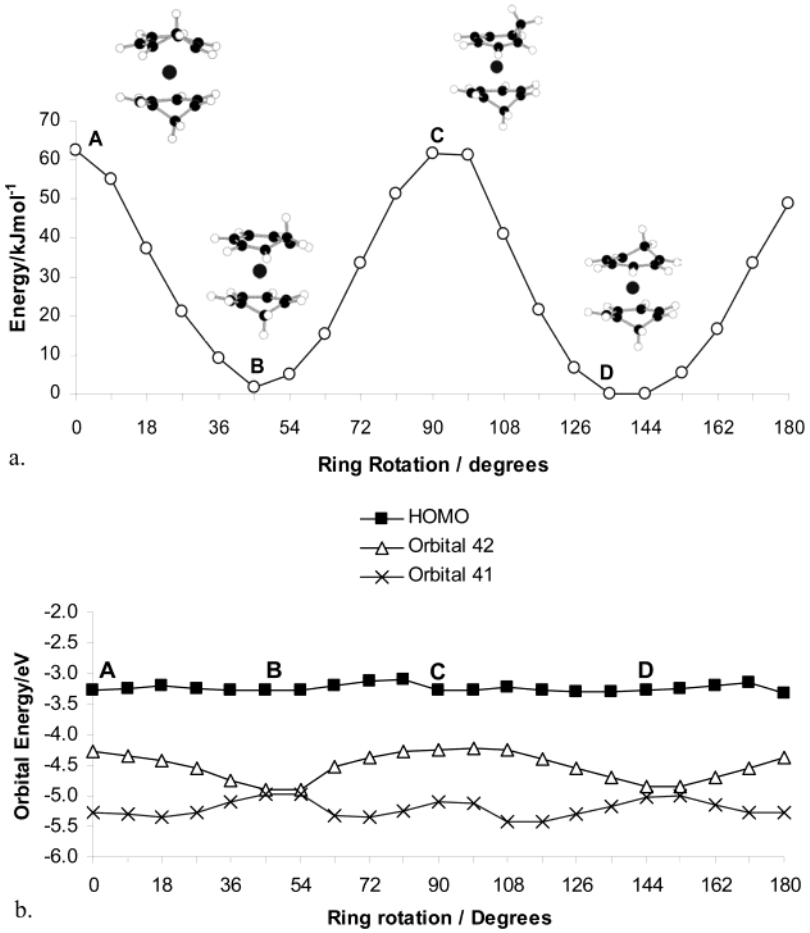

Figure 5. Energy profile for ring rotations of Mo66 through 180°: (a) total energy; (b) energy of occupied orbitals HOMO, orbital 42 (HOMO−1), and orbital 41 (HOMO−2).

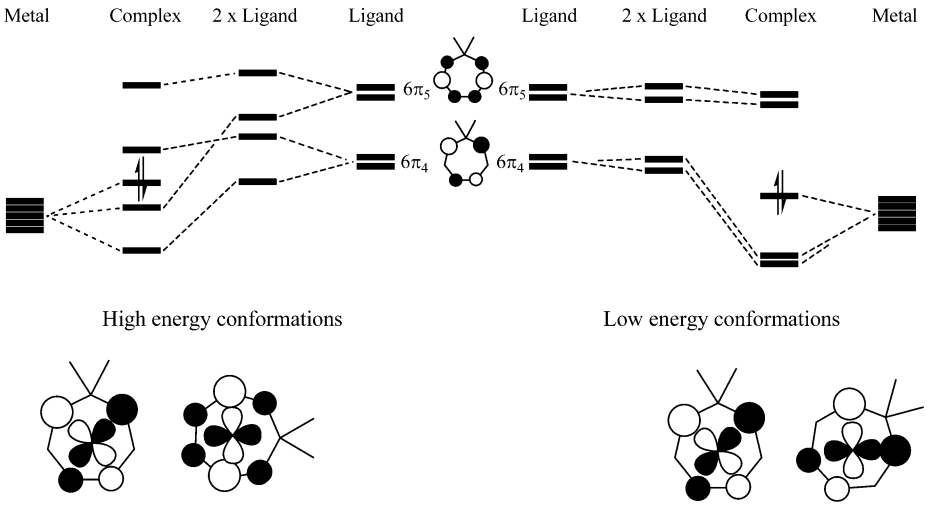

Figure 6. Schematic diagram of the frontier orbitals in Mo66, shown in the high-energy ring conformations (points A and C) and low-energy conformations (points B and D). The HOMO is indicated with two electrons. Shown in the center are the empty ring orbitals of δ-symmetry, which combine and interact with the metal d_{xy} and $d_{x^2-y^2}$ orbitals. In high-energy conformations the unfavorable $6\pi_5$ orbital must be used.

logues of gMo66 and gTS1 with Gaussian, and the results were used with the Eyring equation under the assumption that $\kappa_H/\kappa_D = 1$[46] to give a predicted kinetic isotope effect of 5.4 at 313.5 K, consistent with C−H bond breaking being the highest energy step.

To determine the timing of the process, an IRC calculation using Gaussian was performed from gTS1 and allowed to progress to the minima it connects. Using the results from the IRC, the evolution of selected bond lengths and change in electronic energy in the conversion of Mo66 into Int1 are plotted in Figure 8a. In the initial stage of the reaction decoordination of two

(46) Carpenter, B. K. *Determination of Organic Reaction Mechanisms*; Wiley-Interscience: New York, 1984.

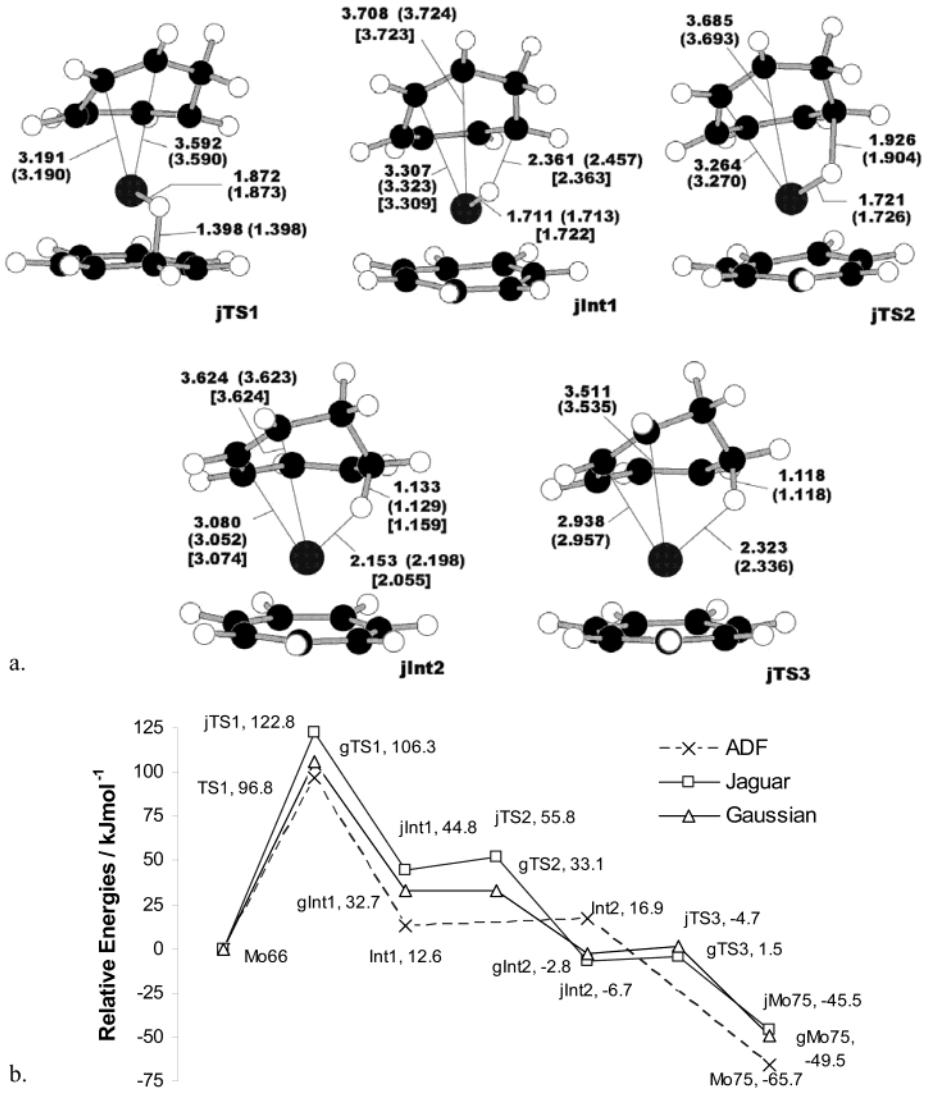

Figure 7. (a) Stationary points in the conversion of Mo66 to Mo75, characterized with Jaguar. Distances shown in parentheses are taken from the Gaussian structures, and those in square brackets are from ADF structures. Distances are marked to the migrating hydrogens and the decoordinated carbons. (b) Relative free energies for the stationary points for the conversion for ADF, Jaguar, and Gaussian. The ADF data from TS1 are obtained using the gTS1 structure and do not represent the true transition state.

carbons from the upper ring occurs. It is also notable that the Mo−C_1 and Mo−C_2 bond lengths have lengthened to about 3 Å before the Mo−H distance begins to reduce. This suggests the ring slippage occurs before the hydrogen approaches the molybdenum center, ensuring the electron count on the metal does not exceed 18. The data plotted in Figure 8a show the C−H bond does not lengthen significantly until very close to the transition state, when the Mo−H distance has reached approximately 2 Å. After the transition state the C−H bond is fully broken, the C_7 ring becomes planar, the Mo−H bond forms, and the two decoordinated carbons move further from the metal.

As formation of Int1 is rate determining, understanding what the barriers are to its formation are key to understanding the observed differences between Mo and Mo^+. To determine how the orbital energies varied during the process, single-point energy calculations were performed on geometries every 2.5 $amu^{1/2}$ bohr, and the resultant orbital energies of the top six filled orbitals are plotted in Figure 8b.

Throughout the reaction pathway there is considerable reorganization of the orbital pattern; however, certain features may be identified. The HOMO remains nonbonding until the transition state. Decoordination of the upper ring carbons results in a rise in energy of orbitals 38 and 40. Of the δ symmetry orbitals, 42 transforms into back-donation to the upper ring and rises slightly in energy at the transition state. Orbital 41, on the other hand, comes to bind mainly to the lower ring, and, as the lower ring becomes more planar, it facilitates a much more favorable interaction with the empty π_4 orbital; this lowers its energy relative to orbital 42, an energy difference that is conserved into Mo75. Orbital 39 stabilizes dramatically over the transition state, lowering by 1.1 eV in the change from gMo66 to gInt1. Initially it is a π bonding orbital deriving from $6\pi_3$, which develops more directional bonding to the lower ring as the upper ring decoordinates. The hydrogen approaching the metal center lies in a nodal plane of the orbital until very close to the transition state. At the transition state hydrogen has moved out of this

Table 3. Corrections to the Relative Energies in the Rate-Determining Transition States[a]

program	GGA energy	larger basis set	ZPE corrected	free energy	solvent corrected
TS1					
ADF	129.7		116.5	103.1	96.8
Jaguar	161.5	149.0	133.0	131.4	122.8
Gaussian	156.7	145.4	129.8	112.9	106.3
TS1+					
ADF	152.7		137.2	121.6	114.4
Jaguar	176.3	166.8	149.3	147.5	135.9
TS4					
ADF	162.4		146.8	127.9	124.7
Jaguar	179.6	175.5	157.7	154.6	148.2
TS6					
ADF	177.4		162.0	143.1	140.3
Jaguar	210.4	203.3	184.5	182.1	181.7
TS7					
ADF	115.7		102.3	92.6	90.3
Jaguar	141.5	137.3	123.3	127.8	127.8

[a] Values shown are in kJ mol^{-1} and are calculated at 298.15 K in toluene for the neutral species and dichloroethane for the cationic TS1+. Details of the corrections can be found in the Computational Methods section.

nodal plane, and the orbital generates a very large directional bonding lobe to the hydrogen. The evolution of orbital 39 over the transition state can be seen in Figure 8c, which plots the orbital at −2.5, 0, and +2.5 amu$^{1/2}$ bohr. These orbitals do not indicate all of the origin of the activation barrier for the reaction. A large amount of energy is used in breaking the C−H bond. This is reflected in lower energy orbitals, whose rise in energy correlates closely with the energy drop of orbital 39.

Transformation of Mo66$^+$ into Mo75$^+$. The orbital with a strong preference for parallel rings, orbital 43, is singly occupied in Mo66$^+$, and so ring bending is less unfavorable in the cationic species. However the energy required for a direct transfer was still found to be far higher than the experimentally determined activation energy, and it was ruled out as a possible mechanism in favor of a metal-mediated hydride shift, as observed for Mo66.

A similar pathway with similar intermediates was established for the cationic system. In this case only the first transition state was characterized. The stationary points found in the conversion of Mo66$^+$ into Mo75$^+$ are shown in Figure 9a, with their relative free energies shown in Figure 9b and Table 3. From the energy profile shown in Figure 9b it is clear that formation of jTS1+ is the rate-limiting step, as was found for the neutral complex. The solvent-corrected free energies of activation are 114.4 and 135.9 kJ mol^{-1} in ADF and Jaguar, respectively (at 298.15 K), compared to the experimental activation energy of 111 ± 3 kJ mol^{-1} (at 323 K).[13] The ADF activation energy compares very well with the experimental value; however the important value is the difference between the neutral and cationic complex. The experimental value difference in free energies of activation is 8 ± 6 kJ mol^{-1}, compared to 17.6 kJ mol^{-1} for ADF and 13.1 kJ mol^{-1} for Jaguar. These data agree with experiment, and we can have confidence that our proposed reaction path is correctly describing the system.

The relative energies of jInt1+ and jTS1+ are different from those for the neutral complex, with the molybdenum hydride intermediate clearly being less

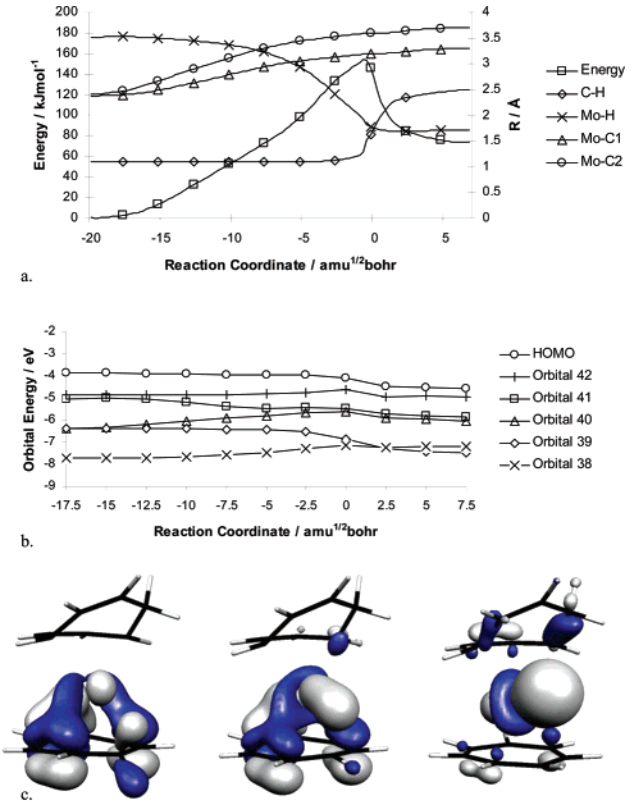

Figure 8. Results of the IRC calculation from Gaussian. The transition state is located at a reaction coordinate of 0. (a) Change in electronic energy (the left axis) and change of selected bond lengths (the right axis) along the intrinsic reaction coordinate between gMo66 and gInt1. Energies are given relative to gMo66. Most data labels are omitted for clarity. (b) Evolution of filled orbital energies obtained from single-point calculations on selected points on the intrinsic reaction coordinates between gMo66 and gInt1. The orbitals are labeled according to their energy levels in Mo66. (c) Evolution of orbital 39 over the gTS1. From top to bottom, orbitals at −2.5, 0, and +2.5 on the IRC. The middle structure represents the transition state.

stable in the cation. Comparing the structure of jTS1+ with jTS1, it is apparent that the cationic transition state lies later on the reaction path. The C−H bond that is breaking is 0.102 Å longer and the Mo−H bond is 0.077 Å shorter in jTS1+ than in jTS1. This would suggest that the cationic molybdenum has contracted orbitals relative to the neutral species. Overlap with the incoming hydrogen is poorer, and hence it must approach closer to the metal center for effective overlap to occur. Poorer metal hydrogen overlap would also explain the relative instablility of jInt1+.

There are however two factors involved in the activation energy, as a large degree of ring slippage to the η^4 structure occurs without significant improvement in metal lower ring interactions. To a reasonable approximation we can determine how this contributes to the total activation energy by reoptimizing the structures of the neutral and cationic complexes with the metal and upper ring fixed at the η^4 geometry of the transition states. This was done in ADF to give activation energies for decoordination of 108.0 and 109.6 kJ mol^{-1} for the neutral and cationic complexes, respectively. Given the approximations involved, these two values cannot be considered as significantly different,

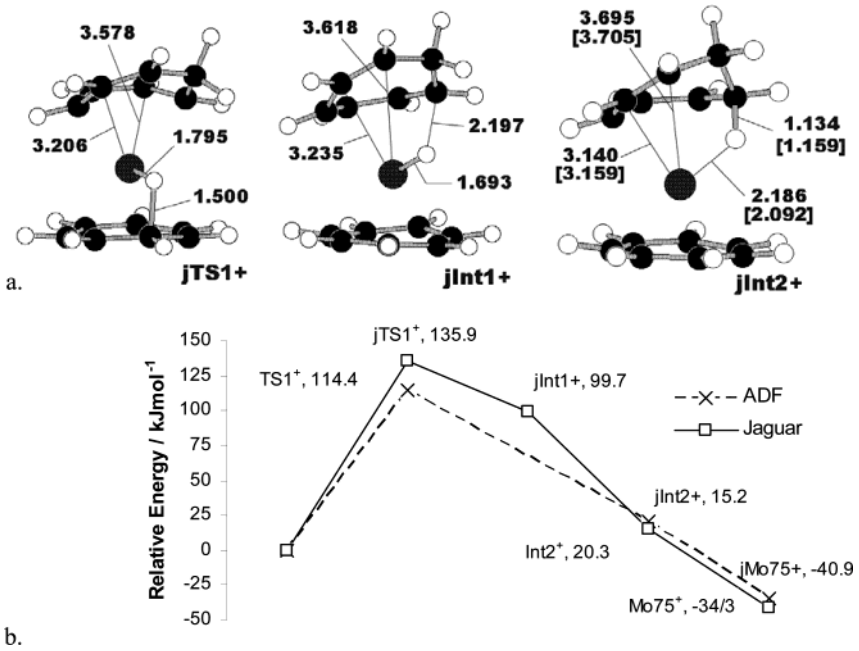

Figure 9. (a) Stationary points found in the conversion of jMo66$^+$ into jMo75$^+$. Distances for ADF stationary points are labeled in square brackets. Distances shown are for the metal to migrating hydrogen, and metal to decoordinated carbon atoms. (b) Relative free energies for the structures shown in (a).

and so we may attribute the difference in activation energies between the neutral and cationic complexes to the differing interaction of the metal with the incoming hydrogen atom and with the lower ring.

A third consideration is that the thermodynamic driving force for the neutral complex rearrangement is greater than for the cation. The extent to which the more favorable binding to the η^7-C_7H_7 ring has formed by the transition state may also be a factor in lowering the barrier for the neutral compound compared to the cation.

Transformation of Zr66 into Zr75. Unlike Mo66, Zr66 is found to be stable to spontaneous rearrangement into Zr75; even after heating at 100 °C in toluene for 48 h there is no significant rearrangement observed, unless a Lewis base is added to the system.[14] The zirconium system was investigated to determine the nature of its stability compared to molybdenum and to determine the mechanism by which a Lewis base facilitates the reaction.

The structures of stationary points found in the conversion of Zr66 into Zr75 are shown in Figure 10a, and their relative free energies in Figure 10b and Table 3. It was found, in the absence of coordinating ligand, that zirconium had two competing mechanisms for the conversion of Zr66 into Zr75. One is analogous to the mechanism found in the molybdenum system, where rate-limiting transfer of a hydride to the metal forms a zirconium hydride intermediate Int4. The second mechanism, via TS6, is a direct transfer without close approach to the zirconium center. Both rate-determining transition states are higher in energy than jTS1 and jTS1+, which agrees with the experimentally observed trend.

An IRC calculation from TS4, and subsequent single-point calculations along the reaction path to analyze the electronic structure, revealed orbital interactions similar to those found in moving across gTS1 (Figure 8b). Again it was found that orbital 39 was the orbital that bonds to the incoming hydrogen, and after the transition state it lowers in energy. However, the stabilization of 0.3 eV of orbital 39 between TS4 and Int4 as compared to 1.1 eV in the molybdenum analogue is indicative of later transition metals forming stronger bonds with hydrogen. The poor binding of zirconium with the incoming hydrogen is reflected in the bond lengths shown in TS4 in comparison with those from TS1 and TS1+. The C−H bond length of the breaking bond is longer in TS4 than TS1 and TS1+, and the M−H distance is closer to the value obtained in the M−H intermediate. The ring hapticities in TS4 are η^6 and η^7, with the upper ring remaining coordinated in the rate-determining step. This occurs as the zirconium hydride intermediate Int4 is 18 electrons, whereas the two extra electrons in molybdenum would make an unfavorable 20 electron configuration if ring slippage did not occur. The structure of TS5 is (η^7,η^4), where ring slippage has occurred to facilitate the hydrogen transfer to the upper ring.

The rearrangement proceeding via TS6 does not involve the metal center so closely. The Zr−H distance does not go below 2 Å, and although there may be some overlap from a diffuse metal orbital, the reaction is considered to be a direct transfer of hydrogen between the two rings. This mechanism has become possible as orbital 43, which increases in energy on ring bending, is empty. This gives both the bent ground state structure of Zr66 as discussed above and a lower barrier to ring bending, which combine to allow TS6 to occur at a more accessible energy.

Experiments show that addition of a Lewis base, such as PMe_3 or CO, facilitates the rearrangement of Zr66 into Zr75.[14] To model the effect of a Lewis base, Zr66 was modeled with PH_3 coordinated to the open face. The ground state geometry showed an inter-ring angle α of 39°. Linear transits were carried out to move the hydrogen between ligands. Moving the hydrogen to the metal was found to be repulsive in energy, and no Zr−H species could be found. A direct transfer transition state

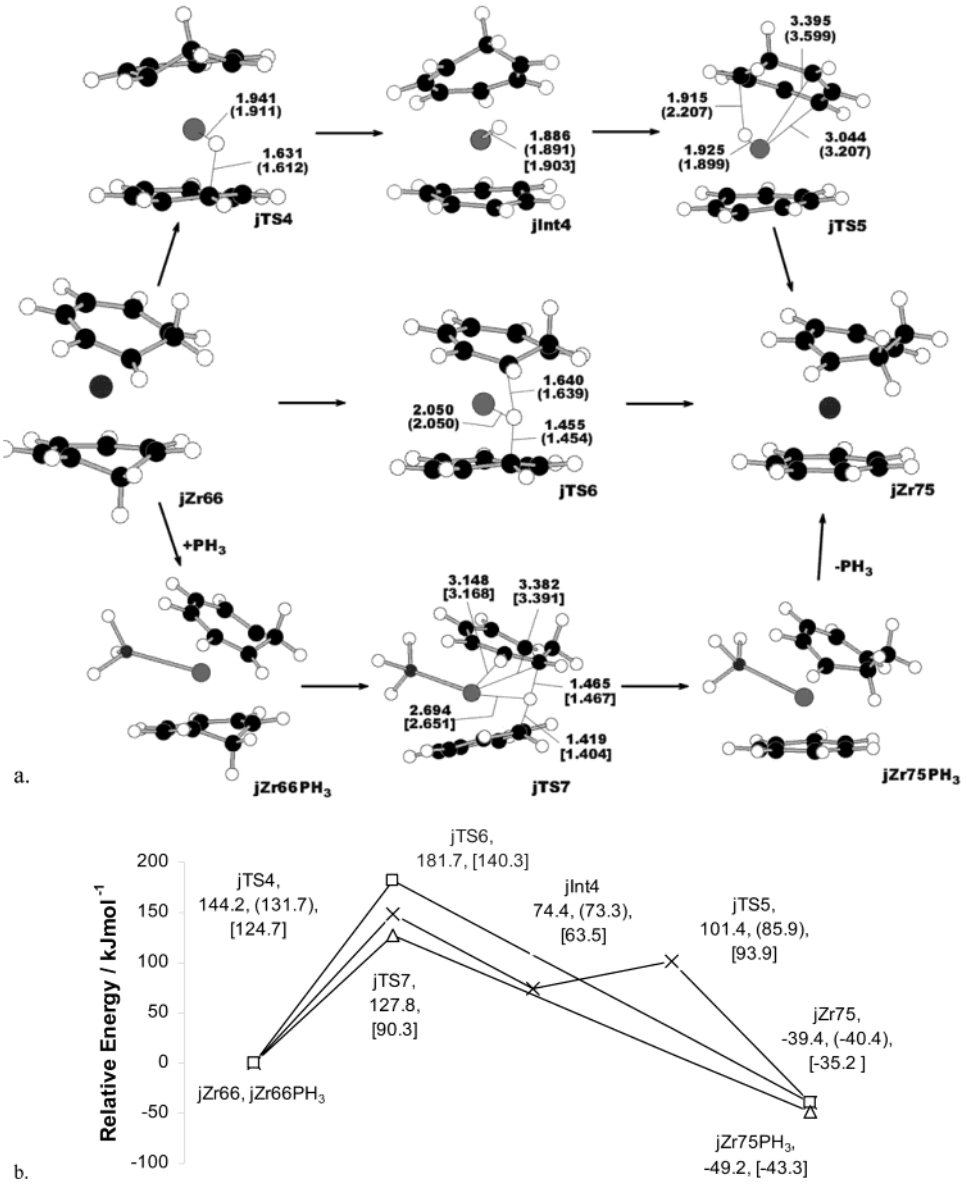

Figure 10. (a) Stationary points found for the conversion of Zr66 into Zr75 using Jaguar. Distances shown in parentheses are taken from the Gaussian structures, and those in square brackets are from ADF structures. Distances are given for the metal to migrating hydrogen, and metal to decoordinated carbon. (b) Relative free energies for the stationary points in the conversion of Zr66 into Zr75. Zr66 and Zr66PH_3 have been set to zero in order to compare the relative barrier heights of the rate-limiting transition states. Gaussian energies are given in parentheses; ADF energies are given in square brackets.

TS7 was found, in which the upper ring has decoordinated an olefin to become η^4, and the migrating hydrogen is placed almost halfway between the two carbons, at ~1.4 Å (Figure 10). Unlike TS6 there is almost certainly no Zr−H interaction, as the Zr−H distance is 2.65 Å, and the mechanism is believed to involve an initial movement of the cycloheptatriene rings to allow a direct transfer to occur.

Figure 10b shows the energy of TS7 relative to the stationary points found for Zr66 to Zr75. It can be seen that adding the Lewis base has reduced the activation energy by ~50 kJ mol^{-1}, which confirms the experimental trend. If we also consider that addition of PH_3 stabilizes the system by 6 kJ mol^{-1}, and so the absolute difference in activation barrier is even more, this further confirms what is observed experimentally. This value of 6 kJ mol^{-1} has two contributing factors: the deformation of Zr66 to open the face up and allow a Lewis base to coordinate ($E_{deformation}$), and the energy released from forming the Zr−P bond (E_{bond}).

$$E_{coord} = E_{deformation} - E_{bond}$$

Our calculations predict that the mechanism by which a Lewis base facilitates the rearrangement is by increasing the inter-ring angle, and hence lowering the activation energy on deforming the system to achieve a direct transfer transition state.

Conclusions

DFT has been used to investigate the electronic structure of the related compounds M(η^6-C_7H_8)$_2$ and M(η^7-C_7H_7)(η^5-C_7H_9) (M = Mo, Mo^+, Zr). Mechanisms for the rearrangement of M(η^6-C_7H_8)$_2$ into M(η^7-C_7H_7)-

(η^5-C_7H_9) (M = Mo, Mo^+, Zr) have been established. The experimental activation energies were well reproduced for Mo and Mo^+. The energy required to increase the inter-ring angle to a suitable geometry for direct transfer of hydrogen made this mechanism prohibitive for Mo and Mo^+. Hydrogen transfer for Mo involved an η^6 to η^4 shift of one ring and the formation of a metal hydride intermediate. Orbital 39 was found to be the primary orbital in bonding to the incoming hydrogen when the C−H bond oxidatively adds to the metal. The decrease in reaction rate as electron count on the metal decreases is a consequence of the poorer binding of the cationic metal to the migrating hydrogen. Rearrangement of Zr(η^6-C_7H_8)$_2$ was found to have two possible mechanisms: a transfer of hydrogen to the metal to form an (η^7,η^6) Zr−H intermediate, and a direct transfer of hydrogen between the two ligands. The metathesis transition state was found to be less favorable. The action of a Lewis base in facilitating the isomerization of Zr(η^6-C_7H_8)$_2$ was reproduced computationally and explained by an increased inter-ring angle upon coordination, giving a lower activation barrier to direct hydrogen transfer via a metathesis-like transition state.

Acknowledgment. We thank the Engineering and Physical Sciences Research Council (EPSRC) for a studentship (B.H.) and the Oxford Supercomputing Centre for the use of their facilities.

Supporting Information Available: Coordinates for all characterized stationary points, the vibrational frequencies, and the thermodynamic analysis. This material is available free of charge via the Internet at http://pubs.acs.org.

OM034292Z